AGU PUBLICATIONS

JGR

Journal of Geophysical Research: Atmospheres

RESEARCH ARTICLE
10.1002/2015JD024556

This article is a companion to *Brown et al.* [2016] doi:10.1002/2015JD024566.

Key Points:
- First observation of $ClNO_2$ in the planetary boundary layer of China
- Combined high-resolution meteorological and measurement-constrained chemical models in data analysis
- $ClNO_2$ enhances daytime ozone peak by 5-16% in well-processed PRD air

Supporting Information:
- Figures S1–S8 and Tables S1–S4

Correspondence to:
T. Wang,
cetwang@polyu.edu.hk

Citation:
Wang, T., et al. (2016), Observations of nitryl chloride and modeling its source and effect on ozone in the planetary boundary layer of southern China, *J. Geophys. Res. Atmos.*, *121*, 2476–2489, doi:10.1002/2015JD024556.

Received 24 NOV 2015
Accepted 19 FEB 2016
Accepted article online 22 FEB 2016
Published online 11 MAR 2016

Observations of nitryl chloride and modeling its source and effect on ozone in the planetary boundary layer of southern China

Tao Wang[1], Yee Jun Tham[1], Likun Xue[2], Qinyi Li[1], Qiaozhi Zha[1], Zhe Wang[1], Steven C. N. Poon[1], William P. Dubé[3,4], Donald R. Blake[5], Peter K. K. Louie[6], Connie W. Y. Luk[6], Wilson Tsui[7], and Steven S. Brown[3,8]

[1]Department of Civil and Environmental Engineering, The Hong Kong Polytechnic University, Hong Kong, [2]Environment Research Institute, Shandong University, Jinan, China, [3]NOAA Earth System Research Laboratory, Chemical Sciences Division, Boulder, Colorado, USA, [4]Cooperative Institute for Research in Environmental Sciences, University of Colorado, Boulder, Colorado, USA, [5]Department of Chemistry, University of California, Irvine, California, USA, [6]Environmental Protection Department, Government of the Hong Kong Special Administrative Region, Hong Kong, [7]PTC International Limited, Hong Kong, [8]Department of Chemistry and Biochemistry, University of Colorado, Boulder, Colorado, USA

Abstract Nitryl chloride ($ClNO_2$) plays potentially important roles in atmospheric chemistry, but its abundance and effect are not fully understood due to the small number of ambient observations of $ClNO_2$ to date. In late autumn 2013, $ClNO_2$ was measured with a chemical ionization mass spectrometer (CIMS) at a mountain top (957 m above sea level) in Hong Kong. During 12 nights with continuous CIMS data, elevated mixing ratios of $ClNO_2$ (>400 parts per trillion by volume) or its precursor N_2O_5 (>1000 pptv) were observed on six nights, with the highest ever reported $ClNO_2$ (4.7 ppbv, 1 min average) and N_2O_5 (7.7 ppbv, 1 min average) in one case. Backward particle dispersion calculations driven by winds simulated with a mesoscale meteorological model show that the $ClNO_2$/N_2O_5-laden air at the high-elevation site was due to transport of urban/industrial pollution north of the site. The highest $ClNO_2$/N_2O_5 case was observed in a later period of the night and was characterized with extensively processed air and with the presence of nonoceanic chloride. A chemical box model with detailed chlorine chemistry was used to assess the possible impact of the $ClNO_2$ in the well-processed regional plume on next day ozone, as the air mass continued to downwind locations. The results show that the $ClNO_2$ could enhance ozone by 5–16% at the ozone peak or 11–41% daytime ozone production in the following day. This study highlights varying importance of the $ClNO_2$ chemistry in polluted environments and the need to consider this process in photochemical models for prediction of ground-level ozone and haze.

1. Introduction

Nitryl chloride ($ClNO_2$) is produced from heterogeneous reaction of N_2O_5 on chloride-containing aerosol [*Finlayson-Pitts et al.*, 1989]. $ClNO_2$ can potentially impact the oxidative capacity of the atmosphere by production of highly reactive chlorine radical (Cl) and recycling NO_x after its photolysis.

(R1) $$N_2O_5(g) + Cl^-(aq) \rightarrow ClNO_2(g) + NO_3^-(aq)$$

(R2) $$ClNO_2 + h\nu \rightarrow Cl + NO_2$$

Subsequent reactions between Cl and volatile organic compounds (VOCs) enhance photochemical formation of ozone via a similar gas-phase mechanism as that for hydroxyl radical (OH) [*Riedel et al.*, 2014; *Sarwar et al.*, 2012, 2014; *Simon et al.*, 2009].

(R3) $$RH + Cl \rightarrow R + HCl$$

(R4) $$R + O_2 + M \rightarrow RO_2 + M$$

(R5) $$RO_2 + NO \rightarrow RO + NO_2$$

(R6) $$RO + O_2 \rightarrow \text{aldehydes/ketones} + HO_2$$

(R7) $$HO_2 + NO \rightarrow OH + NO_2$$

(R8) $$NO_2 + h\nu \rightarrow NO + O\left(^3P\right)$$

(R9) $$O\left(^3P\right) + O_2 + M \rightarrow O_3 + M$$

The abundance of $ClNO_2$ in the ambient atmosphere was first measured by *Osthoff et al.* [2008] on a ship along the Gulf Coast of the U.S., in and around the area of Houston, Texas, and was since detected off the coast of California [*Riedel et al.*, 2012] and in Los Angeles [*Mielke et al.*, 2013]. The presence of $ClNO_2$ in the polluted marine atmosphere arises from strong emissions of NO_x from urban/industrial sources on the coast and of chloride from sea sprays [*Osthoff et al.*, 2008]. Measurements at inland locations have later observed elevated $ClNO_2$ in Boulder, Colorado, (up to 450 parts per trillion by volume (pptv)) [*Thornton et al.*, 2010; *Riedel et al.*, 2013], in Hessen, Germany, (up to 800 pptv) [*Phillips et al.*, 2012], and in London, (up to 724 pptv) [*Bannan et al.*, 2015], whereas moderate levels of $ClNO_2$ (~250 pptv) were observed during a short field study in Calgary, Canada [*Mielke et al.*, 2011]. Two nonoceanic sources—coal-fired power plants and waste-water treatment facilities—are thought to have provided chloride which led to the formation of $ClNO_2$ in Boulder and Calgary, whereas ocean sprays are suggested to be the main source of chloride in London and Germany during the periods of elevated $ClNO_2$.

Due to photolysis of $ClNO_2$ and its precursors (N_2O_5/NO_3) by sunlight, $ClNO_2$ generally shows very low concentrations during daytime, with elevated concentrations typically observed from sunset through early morning in air containing significant amount of O_3 and NO_2, as the result of following gas-phase reactions:

(R10) $$O_3 + NO_2 \rightarrow NO_3$$

(R11) $$NO_3 + NO_2 + M \rightarrow N_2O_5 + M$$

N_2O_5 undergoes heterogeneous reaction (R1) to produce $ClNO_2$ in parallel with hydrolysis of N_2O_5:

(R12) $$N_2O_5(g) + H_2O\ (aq) \rightarrow 2HNO_3(aq\ or\ g)$$

Laboratory and field studies indicate that the product yields of $ClNO_2$ from the N_2O_5 heterogeneous reactions are dependent on the relative content of chloride to that of water in aerosol [e.g., *Mielke et al.*, 2013; *Roberts et al.*, 2009], with field observed $ClNO_2$ yields ranging from 0.07 to 0.98 [*Mielke et al.*, 2011; *Osthoff et al.*, 2008; *Riedel et al.*, 2013; *Thornton et al.*, 2010; *Wagner et al.*, 2013].

The impact of $ClNO_2$ on radical budget, VOC oxidation, and ozone formation have been assessed using chemical box models which are constrained by measurements of $ClNO_2$ and other related parameters [*Bannan et al.*, 2015; *Osthoff et al.*, 2008; *Riedel et al.,* 2014; *Young et al.*, 2012; *Xue et al.*, 2015] or emission-driven chemical transport models. The latter first adopted surrogate gas-phase reaction to represent $ClNO_2$ production [*Simon et al.*, 2009], later the N_2O_5 uptake coefficient derived from ambient observation and assumed $ClNO_2$ yield [*Simon et al.*, 2010], and more recently laboratory-derived parameterization of N_2O_5 uptake and $ClNO_2$ yield [*Sarwar et al.*, 2012; *Sarwar et al.*, 2014]. Box models have found that chlorine atoms from photolysis of $ClNO_2$ contribute to daytime net production of ozone of ~12 ppbv in Los Angeles [*Riedel et al.*, 2014] and 4% of alkane removal on average (up to 15% for the highest $ClNO_2$ case) in London [*Bannan et al.*, 2015]. Recent chemical transport model simulations by *Sarwar et al.* [2014] suggest high concentrations (in the range of parts per billion by volume) of $ClNO_2$ in several regions of the world and enhancement of daily 8 h ozone of up to 7 ppbv, with the largest concentrations and impact in China and western Europe.

Despite the advances achieved in the previous studies, a full picture of global importance of the $ClNO_2$ chemistry is still lacking due in part to limited number of observations of atmospheric abundance of $ClNO_2$ and related chemical and physical parameters in different parts of the world. Up to now, there were only two brief reports of preliminary measurements of $ClNO_2$ in Asia (Hong Kong) [*Tham et al.*, 2014; *Wang et al.*, 2014]. In view of large emissions of NO_x and aerosol in China's polluted regions, it is of great interest to investigate the heterogeneous reactions of N_2O_5 and their role in chorine activation and oxidation processes.

This study presents the measurement results of $ClNO_2$ and related chemical constituents obtained at a mountain top site in Hong Kong during late autumn of 2013. Hong Kong and the adjacent Pearl River Delta (PRD) have long suffered severe pollution from ozone and haze [*Chan and Yao*, 2008; *Wang et al.*, 2009; *Xue et al.*, 2014a]. Large emissions of NO_x, particles, and other anthropogenic pollutants, coupled with the region's proximity to the south China Sea makes it an ideal place to study the heterogeneous formation of $ClNO_2$ and its impact on ozone (and particulate matter). Indeed, in this field study, we observed the highest concentrations ever reported for $ClNO_2$ (and N_2O_5) at one night. This is the first observation of $ClNO_2$ in the upper part of the planetary boundary layer (PBL) over a polluted region of Asia. We first give an overview of the

Figure 1. Google map showing the measurement site (TMS) and surrounding urban areas in Hong Kong and Shenzhen.

$ClNO_2$ results and then examine the chemical characteristics of six high $ClNO_2$ and N_2O_5 cases. High-resolution meteorological model coupled with a backward particle dispersion model is used to reveal the atmospheric dynamics which transports plumes to the mountain top. An explicit chemical mechanism is then employed to evaluate the impact of an extensively processed PRD plume at night on the ozone concentrations in the following day. A companion paper [*Brown et al.*, 2016] analyzes the characteristics of NO_3 and N_2O_5 and their reactions through VOC oxidation and heterogeneous uptake.

2. Methodology

2.1. Field Study Site

The measurements took place at the peak of Mt. Tai Mo Shan (TMS, 22.410°N, 114.125°E; 957 m above sea level), which is the highest point of Hong Kong. As shown in Figure 1, TMS (and Hong Kong) is in the southeast part of the PRD region and is surrounded by major urban areas in Hong Kong and to the south of Shenzhen and other cities of the Guangdong Province. The measurement site is situated in a natural reserve with restricted access to vehicles. The field campaign was conducted from 15 November to 6 December 2013. The instruments are housed in a shelter on the top of TMS.

2.2. Instruments

2.2.1. Chemical Ionization Mass Spectrometry

$ClNO_2$ and N_2O_5 were concurrently measured by an iodide-chemical ionization mass spectrometer (CIMS) (THS Instruments Inc., Atlanta), in which the molecules of interest are ionized to iodide clusters followed by their detection with a quadrupole mass spectrometer. The original configuration [*Slusher et al.*, 2004] (with a heated inlet and detection of NO_3^- at 62 amu) was modified prior to the field study because the previous setup was found to suffer from large interference under high NO_x conditions [*Wang et al.*, 2014]. The modified CIMS adopts an unheated inlet and detects $ClNO_2$ and N_2O_5 as ion clusters, $I(ClNO_2)^-$ and $I(N_2O_5)^-$, as recommended by *Kercher et al.* [2009].

The measurement principle of the CIMS is briefly described here. An alpha radioactive source, ^{210}Po (NRD, P-2031-2000), generates the primary ions, iodide ions (I^-), from CH_3I which is produced by mixing 15 cm^3 min^{-1} STP of CH_3I from a cylinder (0.03% vol/vol in N_2, Arkonic, U.S.) with 1.0 standard liters per minute (sLpm) flow of N_2 (purity: 99.999%). Iodide-water cluster ions are firstly formed ((R13)) then ionize ambient N_2O_5 and $ClNO_2$ ((R14) and (R15)), which are detected as $I(N_2O_5)^-$ at 235 amu and $I(ClNO_2)^-$ at 208 amu.

(R13) $$I^- + H_2O \rightarrow IH_2O^-$$

(R14) $$N_2O_5 + IH_2O^- \rightarrow I(N_2O_5)^- + H_2O$$

(R15) $$ClNO_2 + IH_2O^- \rightarrow I(ClNO_2)^- + H_2O$$

Ambient air was drawn through a 6 m FEP-Teflon tubing (0.25 inch OD) at a total flow of 10 sLpm. The sample inlet was set at 2 m above the shelter roof and is about 6 m above the ground level (see Figure S1 in the supporting information (SI)). The total residence time was less than a second. Only 1.8 sLpm were drawn into the instrument through an orifice, while the rest of the flow was dumped. To reduce uptake of sampled air on particles deposited in the sampling system, a "new" sampling line was used every day. The used tubing and fittings were repeatedly washed with detergent (Decon90), ethanol (Sigma-Aldrich, 99.8%), and ultrapure deionized water under ultrasonic bath (50°C) and then oven dried overnight prior to usage. On-site tests showed that this practice limited the loss of N_2O_5 on the particles to about 10%.

The potential interferences at 235 amu and 208 amu were determined during measurements for 5 min each hour through bypassing the ambient air into a 25 cm length of 0.5 inch OD stainless steel tubing which was packed with stainless-steel wool and heated at 200°C [*Kercher et al.*, 2009; *Phillips et al.*, 2012]. At sampling flow rate of 1.8 sLpm, the residence time of the ambient air in the zeroing tube was ~0.7 s. Laboratory tests show that this zeroing method has removed >98% of N_2O_5 and $ClNO_2$. Figure S2 shows an example of the mass spectrum for ambient samples and for the zeroing period. The sensitivities of the CIMS toward N_2O_5 were determined by the standard addition method. Specifically, a 2.5 ppbv N_2O_5 standard was added in the ambient samples at the top of the inlet for 10 min every 3 h to determine and correct for the changes in sensitivity due to variations of ambient conditions, especially changes in humidity. The N_2O_5 standard was produced by reacting NO_2 in excess with O_3 [*Bertram et al.*, 2009] in a perfluoroalkoxy-made chamber. The concentrations of the produced N_2O_5 were calculated from decrease in NO_2 concentrations [*Wang et al.*, 2014]. To check potential loss of N_2O_5 via productions of nitric acid on surfaces in the calibration system, we measured NO_y output with and without a Nylon filter (pore size = 0.02 μm; Pall Corp.) which would absorb HNO_3 gas. The results did not show any detectable difference in the two setups suggesting little production of HNO_3 from N_2O_5. The N_2O_5 content was also determined during the present field study by a Cavity Ring Down Spectrometer (CRDS) [*Dubé et al.*, 2006; *Wagner et al.*, 2011]. The two methods (i.e., calculation from the NO_2 decrease and quantification of the produced N_2O_5) gave similar N_2O_5 concentrations from the N_2O_5 source (difference < 3%).

The sensitivities of $ClNO_2$ were determined every 2 days by dilution of a $ClNO_2$ standard with humidified dry zero air. $ClNO_2$ was produced by flowing 150 cm^3 min^{-1} STP of known concentration of N_2O_5 through a 0.5 inch OD Teflon tubing (length = 25 cm) quarter filled with slurry of sodium chloride (NaCl). The NaCl slurry was prepared by adding a small amount of ultrapure deionized water (~3 mL) into 1 g of solid NaCl (Sigma-Aldrich, ≥99.8%) producing saturated mixtures. The conversion efficiency of N_2O_5 to $ClNO_2$ on the deliquesced NaCl was shown to be unity [*Finlayson-Pitts et al.*, 1989; *Roberts et al.*, 2009]. The loss of the produced $ClNO_2$ in the system were presumed negligible since its uptake on the water or neutral NaCl slurry is inefficient [*Rossi*, 2003; *Roberts et al.*, 2008].

The N_2O_5 and $ClNO_2$ detections in our configuration show dependence on humidity, similar to other CIMS [*Kercher et al.*, 2009; *Mielke et al.*, 2011]. Results of laboratory tests for our CIMS are given in Figure S3 to show sensitivity as a function of the relative humidity (RH) in the range of 0–90%. It shows that the sensitivity for both N_2O_5 and $ClNO_2$ increases with increasing of RH, reaches the highest at 50%–70% of RH and then decreases. The standard addition method for N_2O_5 calibration has taken account of this humidity dependence at the time of calibration (every 3 h). The changes of sensitivity between the calibrations were corrected based on concurrent measurements of ambient RH and the test result (Figure S3a). $ClNO_2$ was calibrated at a fixed RH of 45%, and the sensitivity during the measurement period was corrected from

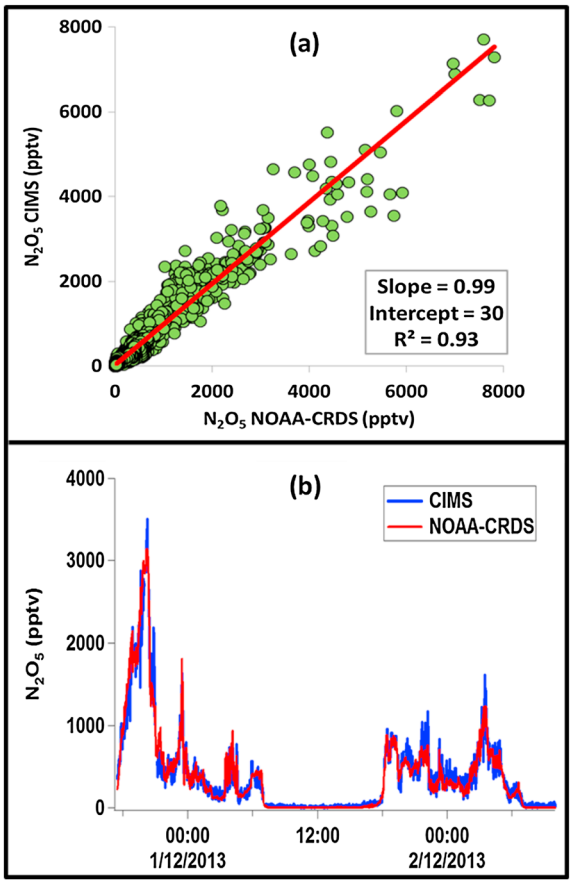

Figure 2. (a) Scatterplot between 1 min averaged N_2O_5 mixing ratios from the NOAA-CRDS (*x* axis) and from the CIMS (*y* axis) for 12 days ($N = 9148$). Solid line (red) represents a RMA linear fit and (b) an example of N_2O_5 mixing ratios from CIMS and CRDS during nighttime and daytime.

the humidity measurements and the test result (Figure S3b). The ambient RH during the measurement period mostly falls in the optimal range.

The detection limit of the instrument was estimated to be 4 pptv for N_2O_5 and 2 pptv for $ClNO_2$ (1σ, 1 min averaged data), with a precision of about 10% and an accuracy of ±20%. The CIMS instrument was not at its optimal operating conditions during the field study due to a degraded radioactive source.

Further verification of the ambient measurements of N_2O_5 by the CIMS was performed by comparing the results with those from the NOAA-CRDS. Figure 2a shows the scatterplot of the data from the two instruments based on the 1 min data collected in the 12 days, and Figure 2b gives the time series of the data for 1–2 December. Overall, an excellent agreement is found, with a correlation coefficient (R^2) of 0.93, a slope of 0.99, and an intercept of 30, based on a reduced major axis (RMA) regression. We also made sure that the measured signal at 208 amu was $ClNO_2$ by examining the correlation with its isotopic ion at 210 amu ($I^{37}ClNO_2^-$). The slope of the correlation was 0.33 ($R^2 = 0.96$, see Figure S4), which is approximately equal to the expected theoretical value of chlorine isotopic ratio of 0.32.

2.2.2. Other Measurements

2.2.2.1. Trace Gases

Nitrogen oxides (NO and NO_2) were measured with a chemiluminescence instrument (Thermo, Model 42i) equipped with a photolytic converter which is not sensitive to reactive nitrogen compounds other than NO_2 [*Xu et al.*, 2013], and total reactive nitrogen (NO_y) was determined by another chemiluminescence analyzer (Thermo, Model 42i) with an externally attached molybdenum oxide (MoO) catalytic converter. The whole air samples were collected hourly during the daytime on selected days with evacuated electropolished stainless steel canisters. The canisters were later shipped to the University of California, Irvine, laboratory for chemical analysis of methane and nonmethane hydrocarbons [*Blake et al.*, 1994; *Simpson et al.*, 2010]. Nitrous acid (HONO) was measured with a long path absorption photometer instrument (QUMA, Model LOPAP-03) [*Xu et al.*, 2015; *Zha et al.*, 2014]. Ozone (O_3) was measured by a UV photometric analyzer (Thermo, Model 49i), while carbon monoxide (CO) and sulfur dioxide (SO_2) were measured by Airpointer compact monitoring system (Recordum).

2.2.2.2. Aerosol Size and Composition

Particle size distribution and numbers were measured in real-time by an Ultrafine Particle Monitor (TSI Model 3031). It measured at a 10 min interval the count of particles in six size bins, i.e., 20–30, 30–50, 50–70, 70–100, 100–200, and 200–1000 nm, with RH ≤ 50% controlled by a nafion dryer. Aerosol surface areas were calculated based on the particle number and geometric mean diameter in each size bin. For the largest size bin of 200–1000 nm, the geometric mean diameter (GMD) of 447 nm may lead to overestimation in surface area. Our previous measurement of the particle size distribution with more size bins at a suburban site in Hong Kong [*Guo et al.*, 2014; *Xu et al.*, 2015] showed that the surface area-weighted mean diameter for 200–1000 nm particles was around 290 nm, and the surface area contributed by particles larger than 400 nm accounted for less than 15% of the total surface area for most of the time. Therefore, a mean diameter

of 282 nm (GMD for 200–400 nm) was used to determine the aerosol surface area of 200–1000 nm particles in the present work. In addition, the particle diameters were corrected for particle hygroscopicity by growth factors under high relative humidity condition (RH > 50%). The wet diameters of particles were calculated with kappa-Köhler function, with mean kappa values of 0.3 adopted from ambient measurement at a coastal suburban site in Hong Kong [*Yeung et al.*, 2014]. Filter sample was collected twice a day with a Harvard honeycomb denuder filter-pack system (Chemcomb Model 3500) on selected days (during daytime and at night). The collected filters were sent to laboratory for chemical analysis for water-soluble ionic concentrations using an ion chromatography (DIONEX, ICS3000). Details on sampling and laboratory analysis were described in *Nie et al.* [2010].

2.2.2.3. Meteorological Parameters

Ambient temperature, relative humidity, wind speed, and direction were monitored using a relative humidity (RH)/temperature probe and a wind monitor (Gill, UK). The photolysis frequency of NO_2 (J_{NO2}) was obtained using a filter radiometer (Meteorologie consult gmbh, Germany).

2.3. Meteorological and Chemical Models

2.3.1. WRF

A Weather Research and Forecasting (WRF) model was adopted to simulate three-dimensional meteorological fields and the planetary boundary layer heights of the PRD region and southern China.

The WRF model was run in four two-way nested domains, with a grid resolution of 27 km, 9 km, 3 km, and 1 km, covering East Asia, southern China, Pearl River Delta, and Hong Kong, respectively. Each domain has 31 vertical levels from surface to 100 hPa. The selections of parameterization options of *Ahmadov et al.* [2012] were adopted in our study. FNL Operational Global Analysis data set provided by National Center for Environmental Prediction (Available at http://rda.ucar.edu/datasets/ds083.2/) was used to initiate the simulation and to provide the boundary conditions. Nudging-based four-dimensional data assimilation technique in *Zhang et al.* [2015] and 3-hourly surface and sounding observations obtained from China Meteorological Administration (CMA) were used to improve the simulation results.

Validation of meteorological simulations of the WRF was conducted with hourly surface observation data obtained from CMA and the Hong Kong observatory. The mean bias, correlation coefficient, and root-mean-square error between observations and modeling results were computed for temperature, relative humidity, latitudinal, and longitudinal wind speeds (Table S1 in SI). The results show that WRF model satisfactorily simulated the atmospheric conditions during the campaign period.

2.3.2. HYSPLIT Model

A Hybrid Single-Particle Lagrangian Integrated Trajectory (HYSPLIT) model was used to analyze the potential source region of an air mass at a receptor backward-in-time. The model can simulate both trajectory and particle dispersions [*Draxler et al.*, 2014]. Trajectory simulation gives the most probable pathway of the air mass and is suitable for conditions under uniform air flow. The particle dispersion application splits air masses into thousands parcels and track their positions (by releasing particles at a receptor and tracking their positions backward in each hour); hence, the particle dispersion is more suitable to simulate air conditions during abrupt synoptic changes, as in our case. In the present study, the HYSPLIT was driven by the WRF generated hourly meteorological fields and was run 12 h backward in time with 2500 particles released at the location of the measurement site. The hourly positions of these particles during the 12 h period were then used to represent the history of air masses. The combination of the high-resolution meteorological simulations and the adoption of particle dispersion are believed to be a better approach in understanding the wind flows and origin of the air masses than use of regular wind measurements or single trajectories with coarse wind data in our study region, which has complex topography (land and oceans, mountains and flatlands, built-up and forested areas, etc.).

2.3.3. MCM Box Model

A comprehensive chemical box model was utilized to evaluate the potential impacts of $ClNO_2$ on the following day's ozone production. The model was based on the Master Chemical Mechanism version 3.2 [*Jenkin et al.*, 2003; *Saunders et al.*, 2003] but was updated to include the heterogeneous reactions of NO_3 and N_2O_5 and the reactions of chlorine atoms with various primary VOCs, which were not represented in the original Master Chemical Mechanism (MCM) (which only considers reactions of chlorine with alkanes). The updated model contains additional 205 Cl-initiated degradation reactions of all primary alkenes, aromatics, aldehydes, ketones, alcohols, selected organic acids, and nitrates as well as the inorganic chemistry of Cl

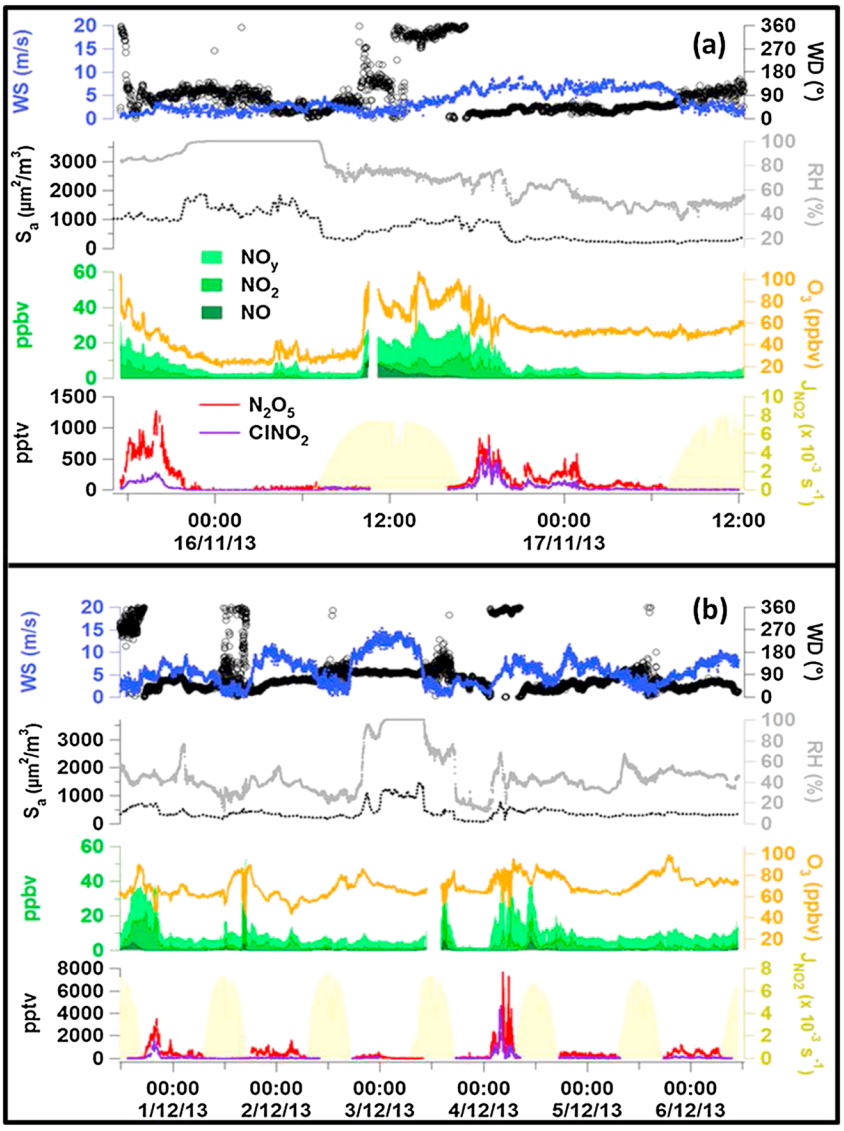

Figure 3. Time series of $ClNO_2$ and related chemical and meteorological parameters of (a) 15–17 November 2013 and (b) 30 November to 6 December 2013.

precursors. The kinetics data are mostly obtained from the IUPAC database. The more detailed description of the model is presented in a separate work [*Xue et al.*, 2015]. The partially updated MCM had been used to assess possible impact of $ClNO_2$ on ground-level ozone with assumed concentrations of $ClNO_2$ [*Xue et al.*, 2014b]. In the present study, constant value of uptake coefficient was adopted: 0.004 for NO_3 and 0.01 for N_2O_5; the latter is consistent with measurement derived value at the site [*Brown et al.*, 2016].

The model was initialized by the observations of O_3, NO, NO_2, HONO, N_2O_5, $ClNO_2$, CO, SO_2, CH_4, C_2–C_{10} non-methane hydrocarbons, and meteorological parameters. The model was run for a 24 h period to simulate the chemical evolution of the prescribed plume after leaving the TMS site. Two scenarios with and without $ClNO_2$ were conducted to examine the impact of reactions of Cl atom with VOCs and of cycled NO_2 from photolysis of $ClNO_2$. The without $ClNO_2$ case simulates the scenario with no $ClNO_2$ produced from the N_2O_5 heterogeneous uptake (i.e., assuming N_2O_5 is converted only to HNO_3 which does not participate in daytime photochemistry in the following day). The difference in the model simulated chlorine atom, OH, HO_2, and ozone concentrations between the two model runs indicate the impact of the $ClNO_2$ photochemistry. The photolysis frequencies were scaled according to the measurements of J_{NO2} at the TMS site. The model was run 5

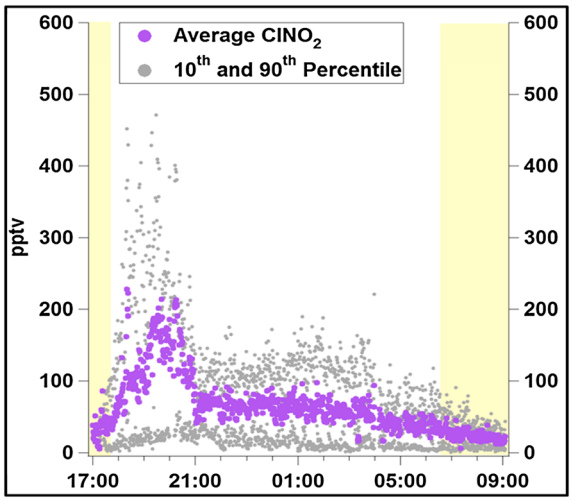

Figure 4. Diurnal pattern of $ClNO_2$ mixing ratios with exclusion of the extreme case of 3–4 December 2013 (purple dots are the means of $ClNO_2$, grey dots represent 90th and 10th percentile).

times to stabilize the unmeasured species (e.g., radicals and reaction intermediates), and the daytime output of the last run was subject to further analysis.

3. Results and Discussion

3.1. Overview of $ClNO_2$ Abundance

During the field campaign, the CIMS had continuous data on 12 days. The data were mostly in nighttime, as the CIMS instrument was under calibration, testing, or maintenance in most of daytime (except weekends). Figure 3 depicts its time series of $ClNO_2$ and some chemical and meteorological parameters relevant to its production and loss on 15–17 November and 31 November to 6 December. The data for the other four nights are not shown because their observations can be represented by the cases in Figure 3 (on 23 and 28 November, the site was consistently immersed within cloud, and the $ClNO_2$ mixing ratios ranged from ~50 to 200 pptv, similar to that of 3 December; on the nights of 25 and 29 November the site received air from the east with $ClNO_2$ ~ 50 pptv, RH ~ 40–60% and low to moderate levels of ozone and other trace gases, similar to 4 December).

Figure 3 indicates that site-intercepted air masses containing elevated levels of $ClNO_2$ (>400 pptv) or N_2O_5 (>1000 pptv) in the evenings (between sunset and 23:59, local time) of 15 and 16 November, 31 November, 1 December, early morning (00:00 to sunrise) of 4 December, the evening of 5 December, and early morning of 6 December. In most of these cases (except for 4 December), the $ClNO_2$ and N_2O_5 levels started to increase after sunset (see Figure 4 for average profile on these days); elevated mixing ratios of ozone (>80 ppbv) and other air pollutants were observed in preceding daytime, and the photochemical "age" of the plume was relatively young as indicated from moderate NO_x to NO_y ratios (~0.4). These observations suggest that the $ClNO_2$ and N_2O_5 in the early evening were produced from NO_x and O_3 emitted/produced in nearby urban areas. The case for 4 December is unique in that (1) the polluted air mass arrived at the site in a much later period of the dark period (3–6 A.M.), (2) 1 min averaged $ClNO_2$, and N_2O_5 mixing ratio reached up to 4.7 ppbv and 7.7 ppbv, respectively, in different periods of this plume, and (3) the air mass was much more aged (as indicated by NO_x/NO_y ratios in Table 1), and the composition showed drastic changes in short periods.

Table 1. Chemical Characteristics of Six High $ClNO_2$ and N_2O_5 Cases

Observation Nights	Duration (Local Time)	N_2O_5 (pptv)		$ClNO_2$ (pptv)					(ppbv)		
		Mean	Maximum	Mean	Maximum	$ClNO_2$:N_2O_5[a]	$(ClNO_2+2N_2O_5)/NO_y$[a]	NO_x/NO_y[a]	O_3[a]	NO_2[a]	NO_y[a]
15–16 Nov	17:50–21:40	575	1278	124	280	0.22	0.098	0.380	52	4.9	13.0
16–17 Nov	17:30–21:00	327	888	181	704	0.55	0.069	0.383	64	4.6	12.0
30 Nov to 1 Dec	17:30–21:00	1729	3498	570	1607	0.33	0.147	0.491	64	13.4	27.3
1–2 Dec	18:11–05:18	573	1648	53	201	0.09	0.146	0.402	60	3.3	8.2
3–4 Dec[b]											
# Plume I	01:40–03:16	1436	2371	637	1358	0.44	0.269	0.174	77	2.3	13.0
# Plume II	03:36–04:13	1619	2261	3212	4700	1.98	0.238	0.154	77	4.2	27.1
# Plume III	04:24–05:55	3675	7707	872	1742	0.24	0.273	0.234	72	7.0	30.1
5–6 Dec	18:26–06:30	374	1237	74	257	0.20	0.107	0.266	73	2.0	7.7

[a]Mean values of the plume.
[b]Extreme case.

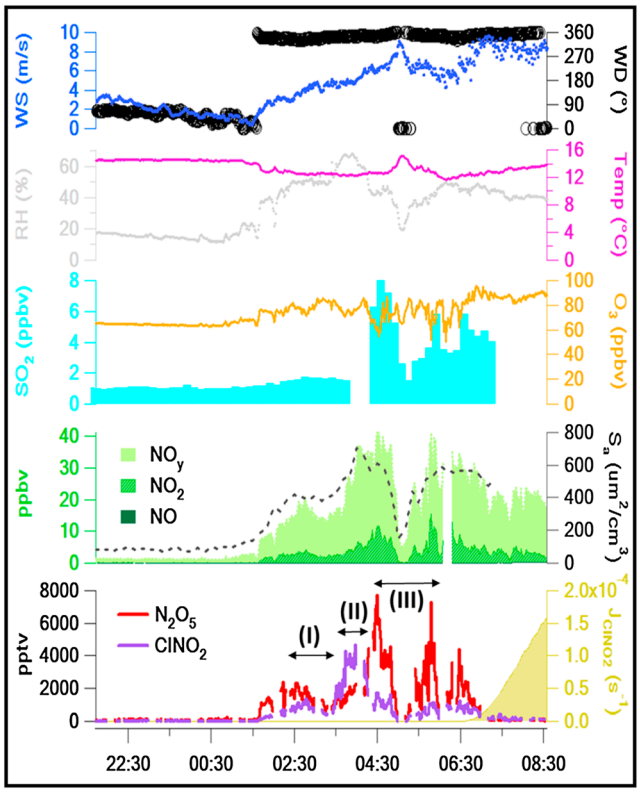

Figure 5. Expanded time series of $ClNO_2$ and related chemical and meteorological parameters for 3–4 December 2013. The arrow indicates Plumes I, II, and III.

Figure 5 depicts the detailed variations of $ClNO_2$ and N_2O_5 and related chemical and meteorological parameters on the night of 3–4 December. Polluted air masses arrived at approximately 02:00. Extremely high mixing ratios of $ClNO_2$ and its precursor, N_2O_5, up to 4.7 ppbv and 7.7 ppbv (1 min averaged), respectively, were seen between 03:30 and 05:00. To our knowledge, such a mixing ratio is the highest value reported in the literature, indicating rapid production of $ClNO_2$ through N_2O_5 heterogeneous uptake in this portion of the plume. Different relationships of these two species were observed between 02:00 and 07:00 (which are labeled as I, II, and III in Figure 5). In Plume I, the two rose almost simultaneously, then Plume II saw a sharp rise in $ClNO_2$ and a slow increase in N_2O_5 (indicating more efficient heterogeneous uptake of N_2O_5), and an opposite pattern followed in Plume III (i.e., high N_2O_5 and low $ClNO_2$, indicative of less efficient uptake of N_2O_5). The aerosol surface area and the relative humidity were the highest in Plume II (see Figure 5). The air masses between 02:00 and 07:00 were well processed chemically with the NO_x/NO_y ratio of 0.17, 0.15, and 0.23 in Plume I, II, and III, respectively.

Table 1 summarizes the chemical characteristics of the six cases of high $ClNO_2$ and N_2O_5. The average mixing ratios for O_3 in these cases were from 52 to 77 ppbv and 2.0 to 13.4 ppbv for NO_2. The mean $ClNO_2$ fraction in NO_y at TMS ranged from 0.006 to 0.118, which is comparable to that observed in Los Angeles and Houston (with the fraction up to 0.15–0.20) [*Mielke et al.*, 2013; *Osthoff et al.*, 2008]. We note that 4 December had the much higher levels of $ClNO_2$ and N_2O_5 but with comparable NO_y and ozone with those for 30 November case. We interpret that the air mass on 4 December had undergone longer periods of processing at night thus accumulated more abundant N_2O_5 and $ClNO_2$. An examination on the composition of the $PM_{2.5}$ sample at this night (18:00–06:00) revealed an abnormal level of chloride. The $[Cl^-]$ to $[Na^+]$ mass ratio was significantly larger than that collected during following daytime (2.48 versus 0.91) and was larger than the mean ratio in sea water (1.8) [*Seinfeld and Pandis*, 2006]. This result indicates the presence of significant amount of nonoceanic chloride in air masses sampled at the night of 4 December. As shown in the following

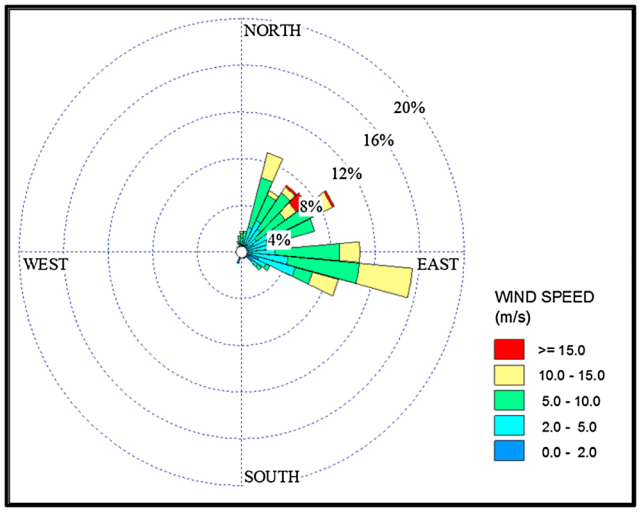

Figure 6. Wind rose of surface wind at the measurement site during this campaign.

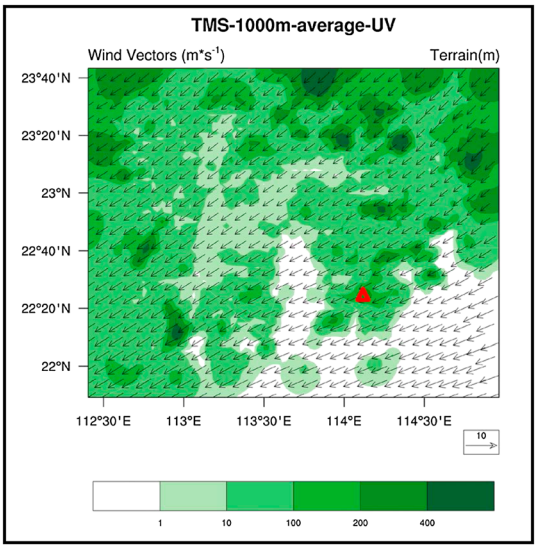

Figure 7. WRF simulated mean wind at 1000 m asl in the PRD.

section, a back trajectory calculation revealed that the aged air mass at the night of 3–4 December came from inland areas of the PRD, suggesting existence of anthropogenic chloride in the PRD region, possibly from coal-fired power plants as indicated by concurrent increase in SO_2 concentrations (Figure 5). Such inference is supported by previous $PM_{2.5}$ aerosol studies conducted in the region, indicative of elevated chloride levels relative to sodium compared to those from ocean sprays [e.g., *Tan et al.*, 2009; *Tao et al.,* 2014]. For example, at an urban site in megacity Guangzhou, which is 120 km north of Hong Kong, the mean concentration for $[Cl^-]$ and $[Na^+]$ is 8.37 μg/m^3 and 2.99 μg/m^3, respectively, in $PM_{2.5}$ samples collected during winter haze periods in 2007/2008, which gives a large $[Cl^-]$ to $[Na^+]$ mass ratio of 2.80. Additional studies are needed to pin down the source(s) of the elevated chloride.

3.2. The Origin of the High $ClNO_2$ and N_2O_5 Air Masses

Figures 6 and 7 show the wind rose at the site and the mean wind field from the WRF simulation during the campaign period. They indicate that the weather of Hong Kong (and the south China coastal regions) in late autumn was strongly influenced by the winter monsoon with winds predominantly from the east and northeast.

To understand the origin of the six high $ClNO_2$ and N_2O_5 cases, we have examined the simulated winds and the 12 h backward-in-time particle dispersion results from WRF and HYSPLIT models (see section 2). The results show that the plumes arriving at the site were associated with changing air flow from the prevailing E/NE to a more northerly direction. Figure 8 shows the result for the 4 December case (other cases are given in Figure S5). At midnight (i.e., before the arrival of the $ClNO_2$ and N_2O_5 plume), the air traveled from the east; but at 04:00 (the middle of polluted air), one branch of air came from the north and from low altitudes, which would bring pollutants from urban areas in Shenzhen and inland areas of the PRD. The enhanced concentrations of SO_2, increased relative humidity, as well as elevated NO_y (see Figure 5) at 04:00 are consistent with meteorological indication of surface air masses. Other cases show similar (but varying) impact of pollution from the north, and the plumes were transported to the site at earlier hours of the night, which means that the air mass had experienced less nighttime processing, consistent with the chemical indicator of age, the NO_x/NO_y ratios (see Table 1). Therefore, based on the above chemical and meteorological analysis, we can conclude that most of the cases of elevated $ClNO_2$ and N_2O_5 are in an early stage of nighttime processing of daytime photochemical pollutants and the

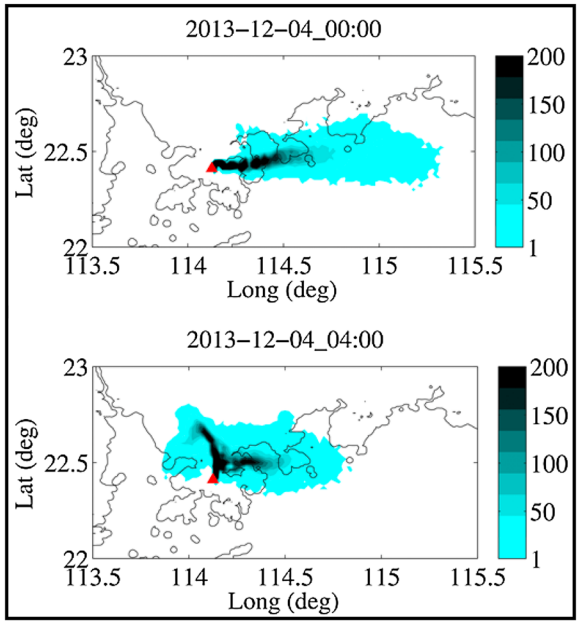

Figure 8. The 12 h backward particle dispersion for 00:00 and 04:00 LT on 4 December 2013. Contours represent the number of particles in each 0.02 latitude × 0.02 longitude grid.

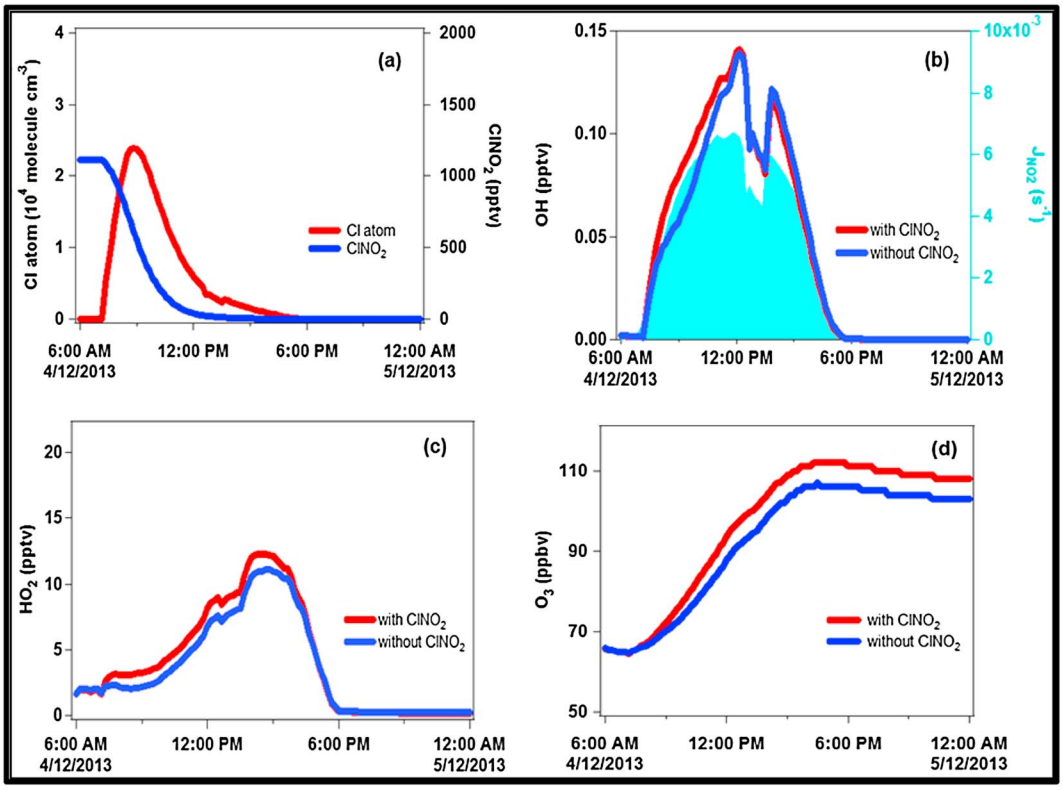

Figure 9. Model simulated concentrations/mixing ratios of (a) $ClNO_2$ and Cl, (b) OH, (c) HO_2, and (d) ozone during the day following plume sampling from the Mt. TMS site, with and without the $ClNO_2$ chemistry. The measured photolysis rate constant of NO_2 is shown by the blue shading. The model was initiated with the measured concentrations of $ClNO_2$ and other relevant chemical constituents at 06:00 (the low $ClNO_2$ case).

4 December case (with the highest $ClNO_2$ and N_2O_5) represents air masses from the PRD region with prolonged nighttime processing. The site intercepted this aged plume as a result of peculiar atmospheric dynamics on that night (i.e., changing wind at a later part of the night). An analysis of a nighttime chemical clock for 4 December based on odd oxygen and discussed in the companion paper [*Brown et al.*, 2016] also suggests a long overnight processing time for plumes sampled during the early hours of 4 December.

3.3. Impact of $ClNO_2$ on Ozone Formation

One important impact of $ClNO_2$ in extensively processed nighttime plumes is its role in photochemistry and ozone production on the following day during air mass transport to downwind locations. The 4 December case provides an opportunity for such an analysis, as the air mass at the night had undergone prolonged processing ($NO_x/NO_y = 0.18–0.23$), and it was measured just a few hours before sunrise. The model was initialized with the $ClNO_2$ concentrations observed 1–3 h before sunrise (see below) assuming no additional $ClNO_2$ production prior to sunrise. This additional production of $ClNO_2$ is difficult to estimate, and we analyze here in terms of the lower limit to the effect on ozone.

To examine whether the $ClNO_2$-rich air was subject to dilution at the sampling height due to growth of the PBL in following daytime, we examined the WRF-calculated height of PBL at five locations over downwind maritime areas (see Figures S6 and S7). It can be seen that the sample location was well above the WRF-calculated height of the PBL at five locations between sunrise (200 m) and noon (600 m). Therefore, $ClNO_2$-driven photochemistry in the sampled air mass residing within the residual layer is not subject to dilution induced by boundary layer growth before noontime. This residual layer O_3 will presumably mix to surface level as the boundary layer grows during afternoon, but our box model simulations are not designed to capture this effect.

We initiated the box model with the chemical data collected in the two periods (1) 3:30–4:00, i.e., with highest abundance of $ClNO_2$ (4.7 ppbv) and moderate level of N_2O_5 (2.15 ppbv), representing a high $ClNO_2$-yield case

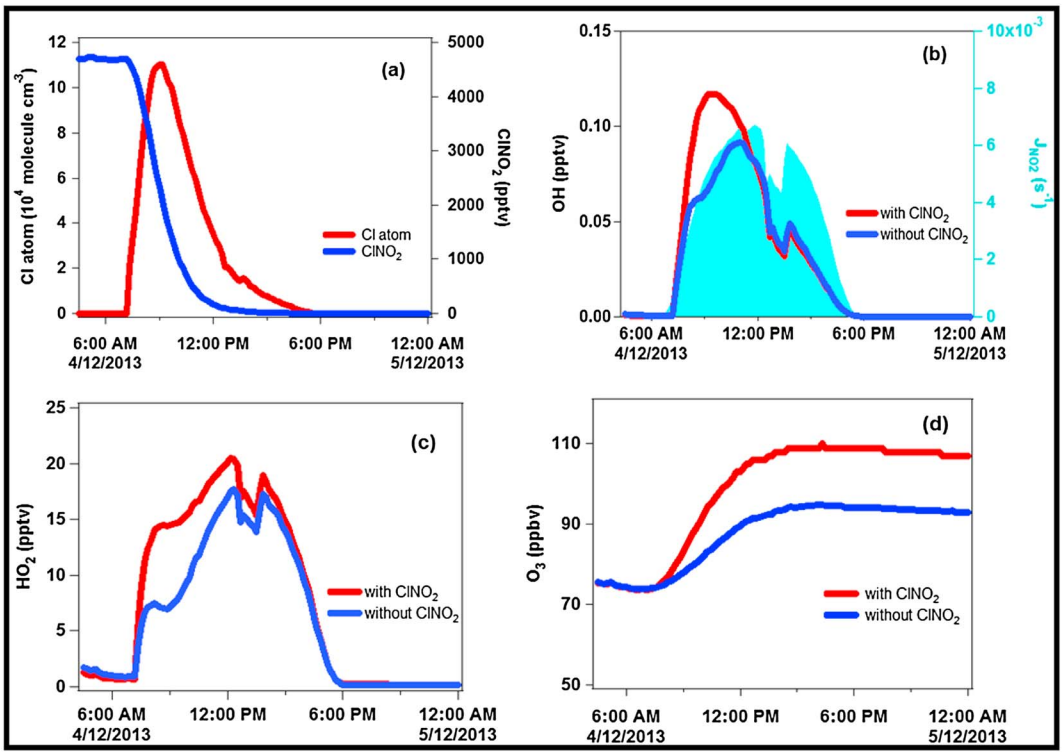

Figure 10. Same as Figure 8, but the model was initiated with the measured $ClNO_2$ and other relevant chemical constituents at 04:00 (the high $ClNO_2$ case).

and (2) 5:30–6:00, a period with very high N_2O_5 (4.96 ppbv) and moderate $ClNO_2$ (1.10 ppbv) representing a low yield case. Table S3 shows the mixing ratios/values of the chemical and meteorological parameters in the simulations of these two cases. As the canister samples for hydrocarbons were collected only during daytime (due to restriction to access the site at night), we estimate the initial hydrocarbons mixing ratios in the simulated night periods according to the following approach. The NO_y mixing ratio at 04:00 was comparable (~40 ppb) to that at 11:00 when a canister sample was collected (see Table S4 for composition). Considering more chemically processed air at 04:00 than at 11:00, as indicated by the NO_x/NO_y ratios of 0.21 versus 0.57, we assume similar abundance of longer-lived alkanes, alkynes, and benzene but only half of the more reactive alkenes and other aromatics in the early morning. We also conducted simulations assuming same, three fourths and one fourth of the reactive hydrocarbon abundance. The oxygenated organics such as aldehydes and ketones were not measured at TMS but were calculated from the measured hydrocarbons by running the MCM model for 5 days [*Xue et al.*, 2014b]. The high $ClNO_2$ case has lower NO_2 (5.0 ppbv) and N_2O_5 levels (2.14 ppbv) compared to the low $ClNO_2$ case (with 9.62 ppbv of NO_2 and 4.96 ppbv of N_2O_5), which means that the chemistry in the former modeling case has lower a NO_x/VOC ratio (because the hydrocarbon abundance is the same in the two cases.)

Figures 9 and 10 show the simulated concentrations of $ClNO_2$, Cl atom, OH, HO_2, and ozone as function of time since the plume left the site for the low and high yield case. Including $ClNO_2$, photolysis resulted in peak concentrations of Cl of 2.4×10^4 molecules cm^{-3} for the low $ClNO_2$ yield case and of 1.1×10^5 molecules cm^{-3} for the high $ClNO_2$ case in the morning period. The Cl reactions with VOCs and the recycled NO_2 have increased the concentrations of OH (via (R7)) and HO_2 (via (R6)) by a maximum of 40% and 53% for the low $ClNO_2$ case and by 77% and 106% for high $ClNO_2$ case, respectively. For the latter case, the integrated OH produced from O_3 photolysis during daytime (6:00–18:00 local time) is 2.0 ppbv; production OH from photolysis of HONO is 3.0 ppbv, with OH produced from $HO_2 + NO$ being 18.5 ppbv. Therefore, in the high $ClNO_2$ case, photolysis of 4.7 ppbv of $ClNO_2$ has contributed nearly 22% of the total radical production during daytime, indicating significant impact on the oxidizing capacity in that air mass.

The effect on peak ozone in low and high $ClNO_2$ yield case is also calculated. For the low $ClNO_2$ case, the peak mixing ratio increased by about 5% (from 99 to 104 ppbv, Figure 9) with lower percentage increases in higher

VOC concentrations (see Figure S8). For the high $ClNO_2$ case, daytime peak ozone increased from 95 ppbv to 110 ppbv, or a 15.8% increase (Figure 10). The ozone formation in the high $ClNO_2$ case is not sensitive to different concentrations of VOCs used in the simulations, as it is in a NO_x-limited regime indicated by higher ozone levels with increased NO_2 concentrations. The $ClNO_2$ chemistry accounts for 11% of the total ozone produced (~45 ppbv; defined as the difference between minimum and maxima in Figure 8d) for the low $ClNO_2$ case but 41% for high $ClNO_2$ case (~36 ppbv, see Figure 9d). For comparison, previous model calculations showed enhancement of 9–12 ppbv in daytime O_3 peak off the coast of Houston [*Osthoff et al.*, 2008] and in the Los Angeles outflow [*Riedel et al.*, 2014], but these locations had a lower percentage increase in daytime production of ozone compared to TMS due to much higher nighttime ozone levels (60–70 ppbv) at TMS than those (20–30 ppbv) at the previous ground sites. These results suggest variable and potentially significant role of $ClNO_2$ in the formation of ozone in polluted regions. More studies in lacking regions/periods are warranted in order to get a more complete picture of the effect of $ClNO_2$ on the formation of secondary pollutants in different chemical environments.

4. Conclusion

The first measurements of $ClNO_2$ in the upper planetary boundary layer of polluted regions of China were conducted at the peak of Mt. Tai Mo Shan (957 m asl) in Hong Kong. The results reveal frequent impact of $ClNO_2$ and N_2O_5 plumes on the high-elevation site in early periods of night with peak $ClNO_2$ mixing ratios of 200–1500 pptv (1 min average). The highest ever reported $ClNO_2$ (4.7 ppbv) was observed in the early morning of one night in extensively processed air from major industrial/urban areas of the Pearl River Delta. Model calculations demonstrate significant enhancement of ozone due to the high levels of $ClNO_2$. We believe that similar concentrations and more frequent occurrences may occur in other locations downwind of the PRD pollution sources and in other regions with strong emissions of NO_x-aerosol-Cl, such as the North China Plain (Beijing) and the Yangtze River Delta region (Shanghai). We suggest field measurements and modeling studies be conducted in these regions in order to obtain a full picture of the role of N_2O_5 heterogeneous reactions and chlorine activation in the formation of ground-level ozone and haze in China.

Acknowledgments

The authors would like to thank Much Yeung, Zhou Shengzhen, Gao Yuan, Xu Zheng, and Wang Xinfeng for their support during the campaign and sample analysis, to Liu Qiang and Zhang Li for help in calculation of back trajectories and WRF simulation, to Lv Mengyao, and Hong Kong Observatory for help in providing observational meteorological data. HYSPLIT model is made available by the NOAA Air Resources Laboratory. This work was funded by the Hong Kong Research Grants Council (PolyU 153026/14P) with additional support from the Hong Kong Environmental Protection Department and the Hong Kong Polytechnic University. Steven S. Brown and William P. Dubé acknowledge support from the NOAA Atmospheric Chemistry, Climate, and Carbon Cycle (AC4) Program. Both the data and source code of the revised chlorine chemistry module for the MCM model used in this study are available from the corresponding author upon request (cetwang@polyu.edu.hk). The opinions expressed in this paper are those of the author and do not necessarily reflect the views or policies of the Government of the Hong Kong Special Administrative Region nor does mention of trade names or commercial products constitute an endorsement or recommendation of their use.

References

Ahmadov, R., et al. (2012), A volatility basis set model for summertime secondary organic aerosols over the eastern United States in 2006, *J. Geophys. Res.*, *117*, D06301, doi:10.1029/2011JD016831.

Bannan, T. J., et al. (2015), The first UK measurements of nitryl chloride using a chemical ionization mass spectrometer in central London in the summer of 2012, and an investigation of the role of Cl atom oxidation, *J. Geophys. Res. Atmos.*, *120*, 5638–5657, doi:10.1002/2014JD022629.

Bertram, T. H., J. A. Thornton, T. P. Riedel, A. M. Middlebrook, R. Bahreini, T. S. Bates, P. K. Quinn, and D. J. Coffman (2009), Direct observations of N_2O_5 reactivity on ambient aerosol particles, *Geophys. Res. Lett.*, *36*, L19803, doi:10.1029/2009GL040248.

Blake, D. R., T. W. Smith, T. Y. Chen, W. J. Whipple, and F. S. Rowland (1994), Effects of biomass burning on summertime non-methane hydrocarbon concentrations in the Canadian wetlands, *J. Geophys. Res.*, *99*(D1), 1699–1719.

Brown, S. S., et al. (2016), Nighttime chemistry at a high altitude site above Hong Kong, *J. Geophys. Res. Atmos.*, *121*, doi:10.1002/2015JD024566.

Chan, C. K., and X. Yao (2008), Air pollution in mega cities in China, *Atmos. Environ.*, *42*(1), 1–42.

Draxler, R., B. Stunder, G. Rolph, A. Stein, and A. Taylor (2014), *HYSPLIT_4 User's Guide*, NOAA Air Resources Laboratory, Silver Spring, Md.

Dubé, W. P., S. S. Brown, H. D. Osthoff, M. R. Nunley, S. J. Ciciora, M. W. Paris, R. J. McLaughlin, and A. R. Ravishankara (2006), Aircraft instrument for simultaneous, in situ measurement of NO_3 and N_2O_5 via pulsed cavity ring-down spectroscopy, *Rev. Sci. Instrum.*, *77*(3), 034101.

Finlayson-Pitts, B. J., M. J. Ezell, and J. N. Pitts (1989), Formation of chemically active chlorine compounds by reactions of atmospheric NaCl particles with gaseous N_2O_5 and $ClONO_2$, *Nature*, *337*(6204), 241–244.

Guo, J., et al. (2014), Atmospheric peroxides in a polluted subtropical environment: Seasonal variation, sources and sinks, and importance of heterogeneous processes, *Environ. Sci. Technol.*, *48*(3), 1443–1450.

Jenkin, M. E., S. M. Saunders, V. Wagner, and M. J. Pilling (2003), Protocol for the development of the Master Chemical Mechanism, MCM v3 (Part B): Tropospheric degradation of aromatic volatile organic compounds, *Atmos. Chem. Phys.*, *3*(1), 181–193.

Kercher, J. P., T. P. Riedel, and J. A. Thornton (2009), Chlorine activation by N_2O_5: Simultaneous, in situ detection of $ClNO_2$ and N_2O_5 by chemical ionization mass spectrometry, *Atmos. Meas. Tech.*, *2*(1), 193–204.

Mielke, L. H., A. Furgeson, and H. D. Osthoff (2011), Observation of $ClNO_2$ in a mid-continental urban environment, *Environ. Sci. Technol.*, *45*(20), 8889–8896.

Mielke, L. H., et al. (2013), Heterogeneous formation of nitryl chloride and its role as a nocturnal NO_x reservoir species during CalNex-LA 2010, *J. Geophys. Res. Atmos.*, *118*, 10,638–10,652, doi:10.1002/jgrd.50783.

Nie, W., T. Wang, X. Gao, R. K. Pathak, X. Wang, R. Gao, Q. Zhang, L. Yang, and W. Wang (2010), Comparison among filter-based, impactor-based and continuous techniques for measuring atmospheric fine sulfate and nitrate, *Atmos. Environ.*, *44*(35), 4396–4403.

Osthoff, H. D., et al. (2008), High levels of nitryl chloride in the polluted subtropical marine boundary layer, *Nat. Geosci.*, *1*(5), 324–328.

Phillips, G. J., M. J. Tang, J. Thieser, B. Brickwedde, G. Schuster, B. Bohn, J. Lelieveld, and J. N. Crowley (2012), Significant concentrations of nitryl chloride observed in rural continental Europe associated with the influence of sea salt chloride and anthropogenic emissions, *Geophys. Res. Lett.*, *39*, L10811, doi:10.1029/2012GL051912.

Riedel, T. P., et al. (2012), Nitryl chloride and molecular chlorine in the coastal marine boundary layer, *Environ. Sci. Technol.*, *46*(19), 10,463–10,470.

Riedel, T. P., et al. (2013), Chlorine activation within urban or power plant plumes: Vertically resolved $ClNO_2$ and Cl_2 measurements from a tall tower in a polluted continental setting, *J. Geophys. Res. Atmos.*, *118*, 8702–8715, doi:10.1002/jgrd.50637.

Riedel, T. P., et al. (2014), An MCM modeling study of nitryl chloride ($ClNO_2$) impacts on oxidation, ozone production and nitrogen oxide partitioning in polluted continental outflow, *Atmos. Chem. Phys.*, *14*(8), 3789–3800.

Roberts, J. M., H. D. Osthoff, S. S. Brown, and A. R. Ravishankara (2008), N_2O_5 oxidizes chloride to Cl2 in acidic atmospheric aerosol, *Science*, *321*(5892), 1059–1059.

Roberts, J. M., H. D. Osthoff, S. S. Brown, A. R. Ravishankara, D. Coffman, P. Quinn, and T. Bates (2009), Laboratory studies of products of N_2O_5 uptake on Cl^- containing substrates, *Geophys. Res. Lett.*, *36*, L20808, doi:10.1029/2009GL040448.

Rossi, M. J. (2003), Heterogeneous reactions on salts, *Chem. Rev.*, *103*(12), 4823–4882.

Sarwar, G., H. Simon, P. Bhave, and G. Yarwood (2012), Examining the impact of heterogeneous nitryl chloride production on air quality across the United States, *Atmos. Chem. Phys.*, *12*(14), 6455–6473.

Sarwar, G., H. Simon, J. Xing, and R. Mathur (2014), Importance of tropospheric $ClNO_2$ chemistry across the Northern Hemisphere, *Geophys. Res. Lett.*, *41*, 4050–4058, doi:10.1002/2014GL059962.

Saunders, S. M., M. E. Jenkin, R. G. Derwent, and M. J. Pilling (2003), Protocol for the development of the Master Chemical Mechanism, MCM v3 (Part A): Tropospheric degradation of non-aromatic volatile organic compounds, *Atmos. Chem. Phys.*, *3*(1), 161–180.

Seinfeld, J. H., and S. N. Pandis (2006), *Atmospheric Chemistry and Physics: From Air Pollution to Climate Change*, Wiley, Hoboken, N. J.

Simon, H., Y. Kimura, G. McGaughey, D. T. Allen, S. S. Brown, H. D. Osthoff, J. M. Roberts, D. Byun, and D. Lee (2009), Modeling the impact of $ClNO_2$ on ozone formation in the Houston area, *J. Geophys. Res.*, *114*, D00F03, doi:10.1029/2008JD010732.

Simon, H., et al. (2010), Modeling heterogeneous ClNO2 formation, chloride availability, and chlorine cycling in Southeast Texas, *Atmos. Environ.*, *44*(40), 5476–5488.

Simpson, I. J., et al. (2010), Characterization of trace gases measured over Alberta oil sands mining operations: 76 speciated C_2–C_{10} volatile organic compounds (VOCs), CO_2, CH_4, CO, NO, NO_2, NO_y, O_3 and SO_2, *Atmos. Chem. Phys.*, *10*(23), 11,931–11,954.

Slusher, D. L., L. G. Huey, D. J. Tanner, F. M. Flocke, and J. M. Roberts (2004), A thermal dissociation–chemical ionization mass spectrometry (TD-CIMS) technique for the simultaneous measurement of peroxyacyl nitrates and dinitrogen pentoxide, *J. Geophys. Res.*, *109*, D19315, doi:10.1029/2004JD004670.

Tan, J., J. Duan, K. He, Y. Ma, F. Duan, Y. Chen, and J. Fu (2009), Chemical characteristics of PM2.5 during a typical haze episode in Guangzhou, *J. Environ. Sci.*, *21*(6), 774–781.

Tao, J., L. Zhang, K. Ho, R. Zhang, Z. Lin, Z. Zhang, M. Lin, J. Cao, S. Liu, and G. Wang (2014), Impact of PM2.5 chemical compositions on aerosol light scattering in Guangzhou—The largest megacity in south China, *Atmos. Res.*, *135–136*, 48–58.

Tham, Y. J., C. Yan, L. Xue, Q. Zha, X. Wang, and T. Wang (2014), Presence of high nitryl chloride in Asian coastal environment and its impact on atmospheric photochemistry, *Chin. Sci. Bull.*, *59*(4), 356–359.

Thornton, J. A., et al. (2010), A large atomic chlorine source inferred from mid-continental reactive nitrogen chemistry, *Nature*, *464*(7286), 271–274.

Wagner, N. L., W. P. Dubé, R. A. Washenfelder, C. J. Young, I. B. Pollack, T. B. Ryerson, and S. S. Brown (2011), Diode laser-based cavity ring-down instrument for NO_3, N_2O_5, NO, NO_2 and O_3 from aircraft, *Atmos. Meas. Tech.*, *4*, 1227–1240.

Wagner, N. L., et al. (2013), N_2O_5 uptake coefficients and nocturnal NO_2 removal rates determined from ambient wintertime measurements, *J. Geophys. Res. Atmos.*, *118*, 9331–9350, doi:10.1002/jgrd.50653.

Wang, T., X. L. Wei, A. J. Ding, C. N. Poon, K. S. Lam, Y. S. Li, L. Y. Chan, and M. Anson (2009), Increasing surface ozone concentrations in the background atmosphere of southern China, 1994–2007, *Atmos. Chem. Phys.*, *9*(16), 6217–6227.

Wang, X., T. Wang, C. Yan, Y. J. Tham, L. Xue, Z. Xu, and Q. Zha (2014), Large daytime signals of N_2O_5 and NO_3 inferred at 62 amu in a TD-CIMS: Chemical interference or a real atmospheric phenomenon?, *Atmos. Meas. Tech.*, *7*(1), 1–12.

Xu, Z., T. Wang, L. K. Xue, P. K. K. Louie, C. W. Y. Luk, J. Gao, S. L. Wang, F. H. Chai, and W. X. Wang (2013), Evaluating the uncertainties of thermal catalytic conversion in measuring atmospheric nitrogen dioxide at four differently polluted sites in China, *Atmos. Environ.*, *76*, 221–226.

Xu, Z., T. Wang, J. Wu, L. Xue, J. Chan, Q. Zha, S. Zhou, P. K. K. Louie, and C. W. Y. Luk (2015), Nitrous acid (HONO) in a polluted subtropical atmosphere: Seasonal variability, direct vehicle emissions and heterogeneous production at ground surface, *Atmos. Environ.*, *106*, 100–109.

Xue, L. K., T. Wang, P. K. K. Louie, C. W. Y. Luk, D. R. Blake, and Z. Xu (2014a), Increasing external effects negate local efforts to control ozone air pollution: A case study of Hong Kong and implications for other Chinese cities, *Environ. Sci. Technol.*, *48*, 10,769–10,775.

Xue, L. K., et al. (2014b), Ground-level ozone in four Chinese cities: Precursors, regional transport and heterogeneous processes, *Atmos. Chem. Phys.*, *14*(23), 13,175–13,188.

Xue, L. K., S. M. Saunders, T. Wang, R. Gao, X. F. Wang, Q. Z. Zhang, and W. X. Wang (2015), Development of a chlorine chemistry module for the Master Chemical Mechanism, *Geosci. Model Dev.*, *8*, 3151–3162.

Yeung, M. C., B. P. Lee, Y. J. Li, and C. K. Chan (2014), Simultaneous HTDMA and HR-ToF-AMS measurements at the HKUST Supersite in Hong Kong in 2011, *J. Geophys. Res. Atmos.*, *119*, 9864–9883, doi:10.1002/2013JD021146.

Young, C. J., et al. (2012), Vertically resolved measurements of nighttime radical reservoirs in Los Angeles and their contribution to the urban radical budget, *Environ. Sci. Technol.*, *46*(20), 10,965–10,973.

Zha, Q., L. Xue, T. Wang, Z. Xu, C. Yeung, P. K. K. Louie, and C. W. Y. Luk (2014), Large conversion rates of NO2 to HNO2 observed in air masses from the south China Sea: Evidence of strong production at sea surface?, *Geophys. Res. Lett.*, *41*, 7710–7715, doi:10.1002/2014GL061429.

Zhang, L., T. Wang, M. Lv, and Q. Zhang (2015), On the severe haze in Beijing during January 2013: Unraveling the effects of meteorological anomalies with WRF-Chem, *Atmos. Environ.*, *104*, 11–21.